Finding the Compromise between Brønsted Acidity and Mesoporosity in Hierarchical ZSM-5 Zeolites

Lucie Desmurs, Claudia Cammarano, Gaetan Ramona, Robin Gaumard, Tzonka Mineva, Alexander Sachse, Thomas Cacciaguerra, Didier Cot, Olinda Gimello, Anne Galarneau, et al.

Finding the Compromise between Brønsted Acidity and Mesoporosity in Hierarchical ZSM-5 Zeolites

Lucie Desmurs,[a] Claudia Cammarano,[a] Gaetan Ramona,[a] Robin Gaumard,[a] Tzonka Mineva,[a] Alexander Sachse,[b] J.D. Comparot,[b] Thomas Cacciaguerra,[a] Didier Cot,[c] Olinda Gimello,[a] Anne Galarneau,[a] Vasile Hulea*[a]

[a] *ICGM, Univ Montpellier, CNRS, ENSCM, Montpellier, France*

[b] *IC2MP, Univ Poitiers, CNRS, Poitiers, France*

[c] *IEM, Univ Montpellier, CNRS, ENSCM, Montpellier, France*

Abstract

Mesoporous ZSM-5 catalysts were prepared from a commercial ZSM-5 (Si/Al =15), using a 2-step micelle-templating procedure. By varying the NaOH/Si synthesis ratio in the range of 0.3-0.7, ZSM-5 catalysts with different textural and acidic properties were obtained. Increasing the NaOH/Si ratio in the synthesis gel leads to zeolites that feature reduced number of Brønsted acid sites, but higher mesopore volume which allows for reducing the diffusion path length. In order to assess the best compromise between Brønsted acidity and mesopore volume two test reactions were run. The alkylation of phenol with *tert*-butyl alcohol allowed to evidence the accessibility of bulky molecules to active sites. The esterification of benzyl alcohol with hexanoic acid allowed to probe the specificity Brønsted acid sites in ZSM-5. The best compromise was found for micro-/mesoporous ZSM-5 catalysts prepared with the ratio $0.38 < NaOH/Si < 0.5$.

Introduction

Zeolites are well-known heterogeneous catalysts that find numerous applications in industry.[1,2] Their specific microporous system confers them with unique acidic properties and shape selectivity. However, the extended micropore systems often induces long diffusion path lengths, which negatively affect the catalytic efficiency factors. One industrially particularly relevant zeolite is ZSM-5 (MFI structure), which features a 10-ring channel system.[3]

To overcome the inconveniences induced by the diffusion limitations, zeolites with hierarchical bimodal porosity, e.g. micropores and mesopores, which allow for reducing the

diffusion path length, have been developed during the last decades. An important number of strategies, including hard and soft templating, demetallation, delamination and recrystallization, have been explored for preparing hierarchical zeolites.[4-6] From a catalytic point of view it results as crucial to evaluate the effect of the improved textural properties with respect to the modified acidic properties. So-called "*test reactions*" have often been used for this purpose.[6,7]

Among the different test reactions, those having an industrial relevance have been frequently employed. For example, the conversion of methanol to hydrocarbons has been used for highlighting the positive effect of the hierarchical pore system on the catalytic activity and stability. The chemical transformation of methanol is a complex reaction, which generates both light hydrocarbons and heavy products such as substituted aromatics, naphthenes and coke using medium pore zeolites.[8] The hierarchical zeolites prove for significantly improved catalyst stability compared to the pristine zeolites.[9] Such behavior was attributed to the reduced coke formation rates, due to an improved diffusion of coke precursors from the micropores to the mesopores. A positive impact on the catalyst lifetime was further observed in methane dehydroaromatization[10] and dehydration of glycerol to acrolein[11] over hierarchical ZSM-5.

Reactions involving bulky reagents and intermediates have further been chosen for evaluating the catalytic performances of hierarchical MFI zeolites. An example is the alkylation of aromatics with benzyl alcohol (BA).[12,13] In this case, a good correlation between the BA conversion and the mesoporous volume of the hierarchical zeolites could be established. Christensen *et al.*[14] studied the benzene alkylation with ethylene to form ethylbenzene. Compared to the conventional ZSM-5 zeolite, the hierarchical counterpart allowed for achieving considerably higher conversions and selectivities toward ethylbenzene. The authors correlated the catalytic results with the improved mass transport properties induced by the presence of mesopores. The acetatilzation of cyclohexanone with methanol,[15] the condensation of benzaldehyde with hydroxyacetophenone[16] and the acid-alcohol esterification[17-20] have moreover been explored as test reactions.

In this study, we prepared a series of mesoporous ZSM-5 samples, using a 2-step micelle-templating procedure from a commercial ZSM-5 (Si/Al =15). Nitrogen sorption isotherms at 77 K and corrected t-plot method were used to determine the micro- and mesopore volumes and surface areas of the mesoporous ZSM-5 catalysts. The nature and concentration of their acid sites were analyzed by FTIR/pyridine spectroscopy. The strength of the acid sites was

measured by TPD-NH_3. The accessibility of their acid sites was probed by the phenol alkylation by *tert*-butanol as test reaction. A second test reaction, the esterification of benzyl alcohol with hexanoic acid was carried out with the aim to assess that mesoporous ZSM-5 samples maintained strong Brønsted acid sites inferable by the sole formation of the ester product. The comparison of the results hence allows to assess the best compromise between the increase accessibility of bulky molecules and the remaining strong Brønsted acidity in hierarchical ZSM-5 samples.

Results and discussion

Structural, textural and morphological properties of mesoporous ZSM-5 catalysts

XRD patterns in the range of 5 to 50° 2θ indicate that all mesoporous ZSM-5 catalysts, named ZSM5-MT(x) where x = NaOH/Si ratio in the synthesis gel, preserve MFI crystalline structure (Figure 1) during micelle-templating (MT). However, the peak intensity decreases linearly with x (Figure S1). Additionally, small angle XRD patterns evidence the apparition of peaks at 2θ = 2.1°, 3.6° and 4.1°, which can be attributed to the hexagonal MCM-41 array (Figure 1 and S1).[21] The corresponding unit cell parameter *a* determined from the (100) reflection at 2θ = 2.1° by the Bragg law is: $a = (2/\sqrt{3})d_{100}$ = 4.9 nm. For the sake of comparison, the Al-MCM-41 synthetized from fumed silica features similar XRD peaks, yet slightly broader.

Figure 1.

N_2 sorption isotherms at 77 K of ZSM5-MT(x) catalysts are a combination of type IV and I, characteristic of mesoporous materials, with a capillary condensation regime at p/p_0 ~0.4, typical of cylindrical mesopores of 4.0 nm (Figure 2, Figure S1) with the presence of micropores (nitrogen uptake at low relative pressure values). The N_2 sorption isotherm of the parent ZSM-5 is of type I (Figure 2), characteristic of a pure microporous materials and features a micropore volume of 0.162 mL g^{-1} (Table 1). A slight increase in nitrogen uptake at high relative pressure values (> 0.7) giving rise to a very thin horizontal hysteresis can be observed, which results from intercrystalline adsorption and indicates the nano-sized nature of the sample. This finding is confirmed from SEM, which allows to deduce crystal sizes of approximately 50-100 nm (Figure S2). In ZSM5-MT(x) catalysts, N_2 isotherms exhibit a much larger horizontal hysteresis, which is typical of the cavitation phenomenon (with a

closure point at p/p_0 = 0.47). This indicates the presence of secondary larger porosity or cavities, which are only accessible through the micro- and/or MCM-41 type mesopores of the catalysts. TEM pictures (Figure S3) confirm the presence of cavities. This finding indicates that the interior of the ZSM-5 nanocrystals dissolves during the alkaline micelle-templating giving rise to hollow *nano-boxes* with shell thicknesses that decreases as a function of x (x = NaOH/Si) (shell thickness ~20 and 10 nm for x = 0.38 and 0.5, respectively). SEM images allow to observe that ZSM5-MT(x) with x = 0.3 and 0.38 are formed by nanocrystals, similar to the parent ZSM-5. By revenge, ZSM5-MT(x) with x = 0.8 features flake-like particles and ZSM5-MT(x) with x = 0.5 and 0.7 are formed by a mixture of nanocrystals and flake-like particles (Figure S2). The number of flake-like particles increases with increasing x at the expense of nanocrystals. ZSM5-MT(0.5) features only a small amount of flake-like particles. Moreover, the width of the horizontal hysteresis of N_2 sorption isotherms of ZSM5-MT(x) decreases for x ≥ 0.6 (Figure S1), which is certainly due to the opening of the *nano-boxes*. Hence, we can propose that the flake-like particles (Figure S2) are mainly formed by purely mesoporous MCM-41-like materials, which seems to be confirmed by TEM (Figure S3).

To summarize, the NaOH/SiO2 ratio plays a crucial role in directing the texture and morphology of mesoporous ZSM5-MT(x) during micelle-templating, which can be classified in four categories:

1- ZSM5-MT(0.3), ZSM5-MT(0.38): hollow boxes of ZSM-5 surrounded by a layer of closely attached MCM-41 like phase.

2- ZSM5-MT(0.5): hollow boxes of ZSM-5 with some open windows surrounded by a closely attached layer of MCM-41 like phase, some MCM-41-like phase extends also in between the nanocrystals.

3- ZSM5-MT(0.6), ZSM5-MT(0.7): composites of two distinct phases: hollow boxes of ZSM-5 with some open windows and detached flake-like particles of MCM-41 like phase.

4- ZSM5-MT(0.8): flake-like particles of MCM-41 like phase

t-Plot analyses performed on nitrogen isotherms evidence the presence of microporosity in ZSM5-MT(x),[22] hence nitrogen isotherms are indeed composite isotherms of type I and type IV. The *t*-Plot analysis of Al-MCM-41 presents zero micropore volume, [22] and is thus purely of type IV. The corrected *t*-plot method[22] was applied to calculate the exact micro- and mesopore surface areas and volumes of ZSM5-MT(x) catalysts (Figure 2, Table 1). Whilst the micropore volume and surface area globally decrease with increasing x (i.e. NaOH/Si ratio), the opposite trend is observed for the mesopore volume and surface area. The mesopore volume increases linearly with increasing x. The study of diffusion in mesoporous silica

carried out by the group of Tallarek[23] evidenced that the diffusion coefficients of molecules is a polynomial function of a parameter, λ, which is the ratio of the kinetic diameter σ of the molecule, diffusing into the mesopore, and the mesopore diameter D, $\lambda = \sigma/D$. The examination of this function shows that for $D/\sigma > 10$, the diffusion coefficient increases linearly with the mesoporous volume and that for larger molecules ($2 < D/\sigma < 7$) the diffusion coefficient is proportional to D and to the mesoporous volume. As ZSM5-MT(x) catalysts feature all the same mesopore diameter (4 nm), the diffusion coefficient of molecules (reactants and products) in ZSM5-MT(x) is expected to increase with the mesoporous volume, hence with x.

The decrease of microporous volume is not a linear relationship with x (Figure 2). The micropore volumes and surface areas of ZSM5-MT(x) with x = 0.3 and 0.38 are very close to the one of the parent ZSM-5 sample (Figure 2). For example, for ZSM5-MT(x) with x = 0.30, 0.38 and 0.50, the micropore volume is 0.154, 0.135 and 0.122 mL g^{-1}, respectively, (Table 1) allowing to calculate that 95%, 83%, 79% of the parent ZSM-5 microporosity is maintained. At the same time, mesopore volume increased from 0.128, 0.133 and 0.209 mL g^{-1}, respectively (Table 1). ZSM5-MT(x) with x = 0.38 exhibits similar micropore and mesopore volumes.

Figure 2

Table 1.

Acidity of mesoporous ZSM-5

All ZSM5-MT(x) feature a global Si/Al ratio close to the one observed for the parent ZSM-5. The Si/Al ratio measured by ICP-OES is close to 16 for all samples. The number of Brønsted acid sites in ZSM5-MT(x) catalysts was quantified by pyridine adsorption followed by FTIR. The FTIR spectrum of the parent ZSM-5 presents a band at 3610 cm^{-1}, characteristic of bridging Si(OH)Al hydroxyls at the origin of Brønsted acidity in ZSM-5 (Figure S4). A low intensity band at 3745 cm^{-1} can be ascribed to the contribution of external silanol groups (SiOH) located at the outer surface of the nanocrystals. A further low intensity band at 3660 cm^{-1} is assigned to SiOH groups with H-bonding with extra-framework aluminum (EFAl) species associated to defects in the structure.[24] ^{27}Al MAS NMR confirms the presence of small amounts of EFAl in the parent ZSM-5 and ZSM5-MT(x) (Figure S5). The FTIR spectra of ZSM5-MT(x) presents a decrease of intensity of the 3610 cm^{-1} contribution and an increase in intensity of the band at 3745 cm^{-1} (Figure S4). This hence indicates that some Brønsted acid sites Si(OH)Al are transformed into terminal Si-OH groups during micelle-templating.

For ZSM-5 and ZSM5-MT(x) typical bands at 1545 and 1455 cm^{-1} are observed, resulting from adsorbed pyridinium ions on Brønsted acid sites (BAS) and pyridine coordinated to Lewis acid sites (LAS), respectively (Figure S6). The parent ZSM-5 features BAS concentration of 0.47 mmol g^{-1} (Table 1). For ZSM5-MT(x) catalysts, the number of BAS decreases with x from 0.47 to 0.15 mmol g^{-1} (Figure 3). As comparison, Al-MCM-41 features very few BAS (0.05 mmol g^{-1}) and a majority of LAS (0.21 mmol g^{-1}) (Table 1). The total acidity of Al-MCM-41 is comparable to that of ZSM5-MT(0.7), but the nature of the sites differs with a majority of BAS (0.15 mmol g^{-1}) and few LAS (0.09 mmol g^{-1}).

There is no direct relationship between the number of BAS and the micro- or mesoporous volume of ZSM5-MT(x) (Figure 4). However, two families of ZSM5-MT(x) catalysts can clearly be distinguished. The ZSM5-MT(x) with $0.3 \leq x \leq 0.5$ with higher number BAS (~ 0.27 mmol/g) but lower mesoporous volume and ZSM5-MT(x) with $x \geq 0.6$ featuring higher mesoporous volume but lower number of BAS (~ 0.15 mmol/g). It is to recall that the former corresponds to the majority of *nano-boxes* particles, whereas the latter to the majority of the flake-like particles assigned to MCM-41-like materials.

Figure 3.

Figure 4.

In ZSM-5 catalysts, BAS is proportional to the number of Al in the MFI structure. A linear relationship (Eq. 1) has been established experimentally with ZSM-5 catalysts with different Si/Al ratio from FTIR/pyridine (outgassed at 150 °C) data from this work and from literature results (Figure 5):

$$\text{BAS (mmol/g)} = 7.28\ [Al/(Al+Si)] \qquad (1)$$

It is to note that the experimental relationship is differs from the one expected from the theoretical chemical formula of H-ZSM-5 ($H_xAl_xSi_{96-x}O_{192}.16H_2O$):

$$\text{BAS (mmol/g)} = 15.84\ [Al/(Si+Al)]$$

The difference results from the fact that not all Al in the parent and micelle-templated zeolites feature sufficient acid character. Indeed, although the global Si/Al ratio calculated by ICP-OES is 16 for all ZSM5-MT(x), from equation (Eq. 1), we can calculate for each ZSM5-MT(x) sample the fraction of Al leading to detectable BAS. Hence for ZSM5-MT(x) with x = 0.3, 0.38, 0.5, 0.6, 0.7 presents the same number of BAS as a ZSM-5 with Si/Al = 24, 26, 28, 44, 47, respectively. Hence the first family of ZSM5-MT(x) with $0.3 \leq x \leq 0.5$ features an

acidity equivalent to a ZSM-5 with Si/Al ~30, whereas the second family with $x \geq 0.6$ an acidity equivalent to a ZSM-5 with Si/Al ~50.

Figure 5.

Another important characteristic of ZSM-5 catalysts is the strength of their BAS. ZSM-5 BAS are able to maintain 53% of pyridinium ions at 723 K (Table S1), which is not possible with Al-MCM-41, where almost no pyridinium ions are detected even at 523 K. ZSM5-MT(x) with $0.3 \leq x \leq 0.5$ reveals to feature strong BAS, indeed 0.06-0.10 mmol/g pyridinium ions are maintained at 723 K. ZSM5-MT(x) with $x \geq 0.6$ present little (0-0.03 mmol/g) remaining pyridinium ions at 723 K.

The strength of the acid sites of ZSM5-MT(x) was also probe by TPD-NH_3 and compared to the one of ZSM-5. The spectra of the catalysts present two peaks: a first peak *T1* around 473 K and a second peak *T2* around 693 K (Figure S7, Table 2). The latter is achieved for ZSM-5 and ZSM5-MT(x) with x = 0.3, 0.38; T2 value then decreases with increasing x for $x \geq 0.5$ (Table 2). The strength of acid sites of all ZSM5-MT(x) is higher than the one of Al-MCM-41 showing a *T2* at 523 K.

From these analysis, it results that the ZSM5-MT(x) family with $0.3 \leq x \leq 0.5$ features the best compromise, presenting acidity equivalent to a ZSM-5 with Si/Al = 30 and mesoporosity, favoring diffusion of reactants and products. In particular, ZSM5-MT(0.5), presenting the highest mesoporous volume should be the catalyst with ideal properties. Yet, some Al-MCM-4-like domains have been observed in SEM in ZSM5-MT(0.5) catalyst that might impact its catalytic properties. To verify these assumptions two catalytic test reactions were carried out: the alkylation of phenol by *t*-BuOH to probe the accessibility of bulky molecules and the esterification of benzyl alcohol with hexanoic acid to probe the intrinsic properties of ZSM-5 (strong BAS).

Alkylation of phenol by tert-Butyl alcohol

The first catalytic test reaction used in this study was the alkylation of phenol by *tert*-butyl alcohol (*t*-BuOH) (Scheme 1).[27-32] This Friedel–Crafts alkylation leads typically to *ortho*- and *para*-*tert*-butylphenol (2-TBP and 4-TBP, respectively) and to the more bulky di-*tert*-butylphenol (2,4-DTBP) over acid catalysts. A secondary product, the tert-butylphenyl ether (TBPE), might by detected resulting from the etherification reaction between two *t*-BuOH molecules (O-alkylation product). In the case of the solid catalysts exhibiting geometric void

spaces, such as zeolites, the distribution of the C-alkylated products (2-TBP, 4-TBP, 2,4-DTBP) strongly depends on the pore size and architecture.[27] Thus, 4-TBP was obtained over beta zeolites (interconnected channels of cross section of 0.76 x 0.64 nm), whereas the 2-TBP was achieved as main product over Y zeolites (windows of 0.74 nm) (Table S2). For mordenite (straight channels of section 0.70 x 0.65 nm), 4-TBP and 2-TBP were obtained with a molar 1:1 ratio. The formation of bulky 2,4-DTBP was observed to occur mainly in the supercages of Y zeolite (1.3 nm).

ZSM-5 features two types of interconnected channels: straight channels of ellipsoidal cross section (0.52 x 0.56 nm) and sinusoidal channels of almost circular cross section (0.54 x 0.56 nm). The intersection of the channels gives rise to larger cavities of ~0.8 nm. The dimensions of the products determined by DFT are: 2-TBP (0.573 x 0.68 x 0.43 nm), 4-TBP (0.79 x 0.43 x 0.38 nm) and 2,4-DTBP (0.79 x 0.68 x 0.43 nm). The products 2-TBP and 2,4-DTBP are hence too bulky to diffuse in ZSM-5 channels. They can form in the intersecting cavities, but will remain trapped. Their presence in the reaction medium is solely due to reaction at the external active sites on the surface of the ZSM-5 nanocrystals. The higher mesopore surface area in ZSM5-MT(x) catalysts should thus lead to an increase in the amount of produced 2-TBP and 2,4-DTBP.

Scheme 1.

In this work, the reaction between *t*-BuOH and phenol was carried out in the liquid phase at 393 K, using parent ZSM-5, ZSM5-MT(x) and Al-MCM-41 catalysts with *t*-BuOH/Phenol molar ratio (1:1). The phenol conversion and the 2,4-DTBP selectivity were analyzed after 4 h of reaction (Figure 6). The parent ZSM-5 exhibits a phenol conversion of 60%, while the selectivity to 2,4-DTBP is 10% (Figure 6). The selectivity in 2-TBP (22%) is similar, and as expected from the dimensions of the molecules the major product is 4-TBP (62%). Despite the small crystal size of ZSM-5 nanocrystals (50-100 nm) the phenol conversion and the selectivity of bulky products (2-TBP and 2,4-DTBP) are limited by the low accessibility of acid sites in pristine ZSM-5. For ZSM5-MT(x) catalysts, the presence of mesopores induces a different behavior. Introducing mesopores in ZSM-5 catalysts increase slightly the phenol conversion and enhance the selectivity in 2,4-DTBP by a factor 2 to 3 for all ZSM5-MT(x) (Figure 6). The highest selectivity towards 2,4-DTPB is obtained for ZSM5-MT(x) with x = 0.38 allowing to achieve 70% phenol conversion and 32% 2,4-DTBP. As comparison, for the Al-MCM-41 catalyst, the phenol conversion is 81% and the selectivity 2,4-DTBP is 29% (Figure 6). The selectivity in 2,4-DTBP for ZSM5-MT(x) is comparable to the one of Al-

MCM-41. Such increase in 2,4-DTBP for ZSM5-MT(x) in comparison to parent ZSM-5 can be ascribed to the increased accessibility of the acid sites. These catalytic results indicate that the created mesopores allow to improve the diffusion and mass transfer of the reactants and/or products for the entire ZSM5-MT(x) series. ZSM5-

Figure 6.

2,4-DTBP is a valuable product in the polymer industry and is usually synthesized using an excess of *t*-BuOH (Table S2).[27-32] To identify if ZSM5-MT(0.38) could allow for producing 2,4-DTBP, the reaction was run with an excess of *t*-BuOH (*t*-BuOH:phenol = 3:1) and compared to pristine ZSM-5 and Al-MCM-41. For ZSM5-MT(0.38) with an excess of *t*-BuOH, the conversion of phenol increases from 70 to 81% and the 2,4-DTBP selectivity increases from 32 to 45%. For pristine ZSM-5 similar conversion and selectivity was observed. Suprisingly, for Al-MCM-41 a phenol conversion of 100% and a selectivity in 2,4-DTBP of 90% was achieved. This corresponds to the highest conversion and selectivity for this reaction carried out in these condition in the literature (Table S2 and ref. herein). Hence, 2,4-DTBT formation does not require the presence of BAS and that LAS can act as efficient active sites. The high phenol conversion and selectivity towards the bulky 2,4-DTBP indicates that it is the accessibility, which is the main parameter that effects the reaction output.

To resume, the alkylation of phenol by *t*-BuOH can be used as catalytic test reaction to probe the accessibility to the active sites, yet it does not allow to probe the impact of Brønsted acid sites. Hence, a second catalytic test reaction was carried out; the esterification of benzyl alcohol with hexanoic acid.

Esterification of benzyl alcohol with hexanoic acid

The esterification of benzyl alcohol with hexanoic acid (Scheme 2) is a nucleophilic substitution reaction and is typically catalyzed by BAS.[19,20] Two possible products can be obtained: the smaller ester (by reaction of hexanoic acid with benzyl alcohol) and the bulkier dibenzyl ether (a by-product, obtained through an acid-catalyzed dehydrative condensation between two alcohol molecules). The esterification and etherification are simultaneous reactions.

Scheme 2.

With ZSM-5 catalysts, only the ester is formed (Table S3 and ref. herein). The ether product was not identified in the reaction mixture, indicating that the ether not even formed at the external surface of the crystals. It was reported that the acid sites responsible for the reaction are the BAS inside the pores of the zeolites.[33] It is indeed the pore architecture and the strength of BAS that influence the product selectivity. It was described that using zeolite beta and Y some dibenzyl ether (20 and 15%, respectively)[33] is formed, which was related to their larger pores and presumably to their weaker acid strength of their BAS. The BAS strength of zeolites increases as follows: MOR > ZSM-5 > *BEA ~ FAU-Y >> Al-MCM-41 (strength determined by the position of the highest temperature peak (*T2*) in TPD-NH_3, at 773, 693, 648, 623, 523 K, respectively (Figure S7)).

ZSM-5 cannot accommodate the large dibenzyl ether molecule, and thus hinders its formation. Dibenzyl ether is not formed when the reaction is carried out in the absence of catalyst. The rate-limiting step is the surface reaction between an adsorbed and a bulk molecule. Acid adsorption is required for esterification to proceed with competitive adsorption of benzyl alcohol. The reaction takes place between the acid adsorbed on the zeolite surface, forming an electrophile and benzyl alcohol in the liquid phase. The yield of the ester is governed by the acidity of the catalysts.

The beneficial contribution of mesoporosity in ZSM-5 on the increase of reactants conversion has previously been reported.[34-37] The authors showed that the reaction mechanism for the ester formation involves an acid/alcohol complex adsorbed on the zeolites active sites. Competitive adsorption of alcohol dimers on the same surface inhibits the production of the ester. Additionally, this behavior increases with growing zeolite pore size.

The benzyl hexanoate is rather bulky compared to the size of the micropores in ZSM-5. Hence, its formation in the micropores will affect the mass transfer of the reactants, which may limit the conversion over ZSM-5. A higher conversion was observed on hierarchical ZSM-5[38] due to improvement mass transfer of reactants and products with a benzyl hexanoate selectivity of 99% .[38] Hence, the hierarchical pore structure allows for reducing mass transfer limitations. Over purely mesoporous catalysts as Al-SBA-15 (prepared by post-modification with aluminum isopropoxide), the observed benzyl alcohol conversion was 33%, and selectivity of benzyl hexanoate was 24%.[38] The rather low selectivity can be explained by the absence of strong BAS in Al-SBA-15. The weak acid sites along with large size of the mesopores might favor the formation of bulky side products such as dibenzyl ether rather than benzyl hexanoate.[38]

In the present study, when the esterification reaction is carried out in the presence of the parent ZSM-5, the conversions of benzyl alcohol and hexanoic acid are similar (~ 13%) and only the ester is detected, as expected (Figure 7). As exposed above, the benzyl ether is too bulky to be formed in the ZSM-5 channels, and does not form at the external surface of the crystal, probably due to the strong acid strength of ZSM-5 leading preferentially to ester formation, which explains its absence. In contrast, in the presence of Al-MCM-41, the selectivity to the ester (benzyl hexanoate) amounts to only 36% and that benzyl ether is observed as main product (64%), which compares well to the observations made using Al-SBA-15.[38] As for Al-SBA-15, the amorphous nature of Al-MCM-41 leads to weaker BAS (as proven by FTIR/Pyridine in temperature (Figure S8)). The weak acid sites along with large size of the mesopores (mesopore diameter of 4 nm) favor the formation of dibenzyl ether rather than benzyl hexanoate. Hence most performant ZSM-5 catalysts are expected to achieve high benzyl hexanoate selectivity (~100%) due to the strong BAS and to an increased reactant conversion due to improved mass transfer.

Figure 7.

For the ZSM5-MT(x) catalysts, three different behaviors were observed (Figure 7):

(i) ZSM5-MT(0.3) and ZSM5-MT(0.38), feature an analogous behavior to that observed for the parent ZSM-5, with 100% benzyl hexanoate selectivity and little increase in benzyl alcohol conversion.

(ii) ZSM5-MT(0.5), which achieves higher benzyl alcohol and hexanoic acid conversion compared to ZSM-5, ZSM5-MT(0.3) and ZSM5-MT(0.38) and a benzyl hexanoate selectivity close to 100% (~94%).

(iii) ZSM5-MT(0.6) and ZSM5-MT(0.7), for which the selectivity in benzyl hexanoate decreases to 70-75% with a conversion in benzyl alcohol slightly lower than that of ZSM5-MT(0.5).

Among the ZSM5-MT(x) catalysts, those featuring highest BAS strength (ZSM5-MT(x = 0.3, 0.38) lead to the exclusive formation of the ester. The selectivity in ester then decreases with reducing acid strength of ZSM5-MT(x) catalysts for $x \geq 0.5$ (Figure S8). Al-MCM-41 with the weakest acid sites produces mainly dibenzyl ether (64%). Hence, ZSM5-MT(0.5) allows for achieving the best compromise between benzyl alcohol conversion (25%) and selectivity towards benzyl hexanoate (almost 100%).

The evaluation of the results from the two catalytic test reactions allows to conclude that the most promising ZSM5-MT(x) catalysts are those synthesized with x = NaOH/Si molar ratio in the synthesis gel in the range $0.38 \leq x \leq 0.5$. These ZSM5-MT(x) feature strong BAS as in the parent ZSM-5 and improved intracrystalline diffusion due to the presence of mesopores.

Conclusion

The mesoporous ZSM-5 were prepared by micelle-templating with different NaOH/Si ratios in the synthesis gel. With increasing ratio the micropore volume and surface area decrease, the mesopore volume and surface area increase and the number of BAS decreases. Two families mesoporous ZSM5 could be distinguished: (i) $0.3 \leq$ NaOH/Si ≤ 0.5 featuring similar nanocrystals shape as parent ZSM-5, but presented as hollow *nano-boxes*, and strong BAS corresponding to an acidity of a ZSM-5 with Si/Al = 30, and (ii) NaOH/Si ≥ 0.6 which are a mixture of *nano-boxes* and flake-like particles identified as MCM-41-like material, and featuring weaker BAS. The alkylation of phenol by *t*-BuOH allows to probe the accessibility towards the active sites, but not the strength of the acid sites, whereas the esterification of benzyl alcohol with hexanoic acid permits to identify the best compromise between strong BAS and accessibility (or improvement of mass transfer).

Experimental section

Synthesis of mesoporous ZSM-5

The mesoporous ZSM-5 were prepared via a 2-step micelle-templating (MT) procedure adapted form Goto *et al.*[39] starting from a commercial ZSM-5 (Si/Al = 15). In a typical synthesis, 2.5 g of NH_4-ZSM-5 (CBV3024E Zeolyst, crystal size of about 100 nm) were treated with sodium hydroxide (Sigma-Aldrich) and octadecyltrimethylammonium bromide (C_{18}TAB, Sigma-Aldrich) with the following ratios assuming zeolites in calculation as pure silica: 1 SiO_2: 0.1 C_{18}TAB: x NaOH: 56 H_2O with $0.30 \leq x \leq 0.70$. First, the aqueous solution of NaOH and C_{18}TAB was prepared in a water bath at 50 °C for optimum surfactant dissolution and then the zeolite powder was added under stirring. After dispersion for 20 min, the mixture was poured in a Teflon lined stainless steel autoclave for a 24-hour first step at 383 K followed by pH adjustment at pH 8.5 with 2.0 M HCl solution and a second 24-hour step at 383 K. The solid was recovered by filtration, washed with deionized water until neutral pH, dried overnight at 373 K and calcined 2 h at 623 K and 8 h at 838 K (0.5 K min^{-1}) to

remove the surfactant. The synthetized materials were designated ZSM5-MT(x) with x the NaOH/Si synthesis ratio. The acidic form of catalysts was obtained by ionic exchange with an aqueous 0.1 M NH_4NO_3 solution (100 mL per g solid) at 363 K under reflux for 1 h. The procedure was repeated 3 times with filtration in between, then washed with water (100 mL per g solid), dried at 353 K and calcined at 823 K for 8 h to liberate ammonia and obtain the H^+ form.

Synthesis of mesoporous Al-MCM-41

Al-MCM-41 (Si/Al = 15) was synthesized by mixing water, NaOH, $NaAlO_2$ and C_{18}TAB at 323 K to obtain a clear solution. Then silica powder (2.5 g) (fumed silica, Aerosil 200, Degussa) was added and the mixture was stirred for 20 min. The molar composition of the mixture was: 1 SiO_2: 0.1 C_{18}TAB: 0.25 NaOH: 56 H_2O: 0.066 $NaAlO_2$. The mixture was then transferred into an autoclave and placed in an oven at 388 K for 24 h. The recovered solid was filtered, water washed until neutral *pH*, dried at 373 K for 24 h and calcined under air at 823 K for 8 h.

Material characterization

Crystalline phase and mesoporous order were followed by X-ray diffraction (XRD) on a D8 Bruker device (Cu Kα radiation) in the ranges 2θ = 4 - 50° and 0.5 - 6°, respectively, with a 0.2° angular step. Textural properties were analyzed by N_2 sorption at 77 K. 100 mg of materials were outgassed under vacuum at 523 K for 6 h prior nitrogen sorption analysis at 77 K using a Micromeritics Tristar apparatus. Specific surface area was determined using the BET method. The relative pressure range to use the BET equation $(p/p_0)/[V(1-p/p_0)] = f(p/p_0)$ was determined using the superior limit given by the maximum of the Rouquerol curve $V(1-p/p_0) = f(p/p_0)$.[40] Microporous and mesoporous surfaces and volumes were determined by the corrected t-plot analysis.[22,41] Mesopore diameters were calculated by Broekhoff and De Boer (BdB) desorption method[42] at the inflexion point of the desorption step. Scanning electron microscopy (SEM) images were recorded using Hitachi S-4800 I FEG-SEM at “Plateau Technique de l’IEM laboratoire du Pole Chimie Balard Montpellier”. Transmission electron microscopy (TEM) images were recorded using a JEOL 1200 EX2 microscope operating at 100 kV at “Plateau Technique du Pole Chimie Balard Montpellier”.

Determination of Brønsted and Lewis acidity was performed by FTIR/pyridine on a Nicolet 5700 instrument. The material is first compressed (0.5 T) to form a self-supported pellet (2

cm^{-2}, 10-30 mg) and heated at 823 K under air flow (60 mL min^{-1}). The sample was then outgassed (10^{-5} bar) at 473 K for 1 h before to register the first FTIR spectrum. The sample is cooled at 423 K and exposed to pyridine (1.5 mbar) for 5 min and outgassed (10^{-5} bar) to remove physisorbed pyridine. The quantification of Brønsted and Lewis acid sites was done by integration of the bands at 1545 and 1455 cm^{-1}, respectively, with the following extinction coefficients: ε_{1545} = 1.13 and ε_{1455} = 1.28 cm mol^{-1}. The extinction coefficients were achieved experimentally in previous studies using another ZSM-5 zeolite (without Lewis acid sites) of Si/Al = 27 and a γ-alumina (Lewis acid sites) at 20 °C in a glass cell with KBr windows. The calibration curves were obtained by adding to the IR cell a known amount of pyridine vapor from a gas admission compartment (0.9122 cm^3). Extinction coefficient for ZSM-5 is close to the one determined recently by advanced method by Zholobenko et al.[43].

Acidity of H^+-form of zeolites was probed with NH_3-TPD on a Micromeritics Autochem II with 50 mg of samples. Particles size of the powders was controlled by compressing (2 T) for 1 min 200 mg of powder into pellets of 16 mm diameter with a press SPECAC 15 t and then grinding and sieving the pellets between 150 and 250 µm. First, a 2-hour calcination steps at 550 °C allows sample surface preparation before ammonia adsorption at 373K for 40 min with 5% NH_3 in He. Desorption is carried out with a 25 cm^3/min He flow at 10 °C/min to 600 °C. Temperature ramping starts when TCD signal is stable and desorption of weakly physisorbed ammonia is over. A calibration of TCD signal allows data treatment and calculation of acid site concentration.

Molar ratio Si/Al of the ZSM5-MT(x) was calculated from ICP-OES analysis.

Alkylation of phenol by tert-butanol

The reaction test of phenol alkylation by *tert*-butanol (*t*-BuOH) was performed using a Multi-reactor Parr station. 200 mg of calcined H^+-catalyst was poured with 19 cm^3 of heptane (Sigma-Aldrich), 0.769 g of nonane (internal standard, Sigma-Aldrich), 0.565 g of phenol (PhOH) (99% detached crystals, VWR) and 0.445 g or 1.335 g of *t*-BuOH (VWR) for *t*-BuOH/PhOH = 1 or 3 (mol/mol), respectively. After 4 h at 393 K under 700 rpm, reactors were quenched in cold water and the mixture collected and filtered for injection in a GC6850 Agilent equipped with HP-1 30 m x 250 µm x 0.5 µm column and FID detector. Identification of peaks was done by mass spectroscopy on a GCMS-QP2010 Plus apparatus.

Esterification of benzyl alcohol with hexanoic acid

In a typical reaction, 100 mg of catalyst was introduced into a 25 mL two-necked flask equipped with reflux, magnetic stirring, vacuum pump and nitrogen flow. First, the catalyst

was activated (dehydrated) at 423 K under vacuum for at least 6 h. Then, under an inert atmosphere, 5 mmol of benzyl alcohol (Sigma-Aldrich) and 5 mmol of hexanoic acid (Sigma-Aldrich) were introduced into 2.5 mL of dry toluene. 1 g nonane (Sigma-Aldrich) was used as internal standard. Esterification was carried out for 4 h at 383 K with stirring at 500 rpm. After cooling and centrifugation, the reaction mixture is analyzed by GC. The products were identified by GC-MS (Shimadzu GCMS-QP2010Plus). Quantification of reactants and products was performed on an Agilent GC6850 GC-FID device equipped with a 30 m x 250 µm x 0.5 µm HP-1 column.

References

1. W. Vermeiren, J.P. Gilson, *Top Catal*. **2009**, *52*, 1131–1161.

2. C. Martinez, A. Corma, *Coord. Chem. Rev*. **2011**, *255*, 1558–1580.

3. K. Tanabe, W. Holderich, *Appl. Catal. A: Gen.*, **1999**, *181*, 399-434.

4. J. Pérez-Ramírez, C.H. Christensen, K. Egeblad, C.H. Christensen, J.C. Groen, *Chem. Soc. Rev.* **2008**, *37*, 2530-2542.

5. L.H. Chen, X.Y. Li, J.C. Rooke, Y.H. Zhang, X.Y. Yang, Y. Tang, F.S. Xiao, B.L. Su, *J. Mater. Chem.* **2012**, *22*, 17381-17403.

6. M. Hartmann, A.G. Mackoke, W. Schwieger, *Chem. Soc. Rev*. **2016**, *45*, 3313-3330.

7. C.M.A. Parlett, K. Wilson, A.F. Lee, *Chem. Soc. Rev*. **2013**, *42*, 3876-3893.

8. A. Lacarriere, J. Robin, D. Świerczyński, A. Finiels, F. Fajula, F. Luck, V. Hulea, *ChemSusChem* **2012**, *5*, 1787-1792.

9. J. Kim, M. Choi, R. Ryoo, *J. Catal*. **2010**, *269*, 219-228.

10. N. Chu, J. Yang, J. Wang, S. Yu, J. Lu, Y. Zhang, D. Yin, *Catal. Commun*. **2010**, *11*, 513-517.

11. L.G. Possato, R.N. Diniz, T. Garetto, S.H. Pulcinelli, C.V. Santilli, L. Martins, *J. Catal.* **2013**, *300*, 71-79.

12. X. Zhang, D. Liu, D. Xu, S. Asahina, K.A. Cychosz, K.V. Agrawal, Y. Al Wahedi, A. Bhan, S. Al Hashimi, O. Terasaki, M. Thommes, M. Tsapatsis, *Science* **2012**, *336*, 1684-1687.

13. G. Song, W. Chen, P. Dang, S. Yang, Y. Zhang, Y. Wang, R. Xiao, R. Ma, F. Li, *Nanoscale Res. Lett*. **2018**, *13*, 364.

14. C.H. Christensen, K. Johannsen, I. Schmidt, C.H. Christensen, *J. Am. Chem. Soc*. 2003, *125*, 13370-13371.

15. J. Lin, M.O. Cichocka, F. Peng, T. Yang, J. Sun, *Chem. Eur*. **2018**, *24*, 14974-14981.

16. F. Liu, T. Willhammar, L. Wang, L. Zhu, Q. Sun, X. Meng, W. Carrillo-Cabrera, X. Zou, F.S. Xiao, *J. Am. Chem. Soc*. **2012**, *134*, 4557-4560.

17. M. Milina, S. Mitchell, J. Pérez-Ramirez, *Catal. Today* **2014**, *235*, 176-183.

18. Y. Yang, W. Jiang, J. Jiang, Q. Qiu, P. Mao, M. Wu, *J. Solid State Chem.* **2020**, *292*, 121686.

19. R.R. Mukti, Y. Kamimura, W. Chaikittisilp, H. Hirahara, A. Shimojima, M. Ogura, K.K. Cheralathan, S.P. Elangovan, K. Itabashi, T. Okubo, *ITB J. Sci.* **2011**, *43 A (1)*, 59–72.

20. A. Corma, H. Garcia, S. Iborra, J. Primo, *J. Catal.* **1989**, *120*, 78–87.

21. C. Kresge, M. Leonowicz, W.J. Roth, J.C. Vartuli, J.S. Beck, *Nature* **1992**, *359*, 710–712.

22. L. Desmurs, A. Galarneau, C. Cammarano, V. Hulea, C. Vaulot, H. Nouali, B. Lebeau, T.J. Daou, C. Vieira Soares, G. Maurin, M. Haranczyk, I. Batonneau-Gener, A. Sachse,

ChemNanoMat **2022**, *8*, e202200051.

23. S.J. Reich, A. Svidrytski, D. Hlushkou, D. Stoeckel, C. Kubel, A. Holtzel, U. Tallarek,

Ind. Eng. Chem. Res. **2018**, *57*, 3031-3042.

24. H.J. Mesa, A.C. Faro Jr, V.O. Rodrigues, *J. Braz. Chem. Soc*., **2021**, *32*, 1193-1202.

25. Y-L. Ye, M. Fu, H. Chen, X. Zhang, *J. Fuel Chem. Technol*. **2020**, *48*, 311-320.

26. D. Kertens, H. De Peuter, I. Khalil, S. Van Praet, J. Van Aelst B.F. Sels, *ACS Sustainable Chem. Eng.* **2021**, *9*, 4357-4362.

27. E. Dumitriu, V. Hulea, *J. Catal*. **2003**, *218*, 249–257.

28. E. Dumitriu, D. Meloni, R. Monaci, V. Solinas, *C.R. Chimie* **2005**, *8*, 441-456.

29. E. Modrogan, M.H. Valkenberg, W.F. Hoelderich, *J. Catal*. **2009**, *261*, 177–187.

30. A. Ungureanu, B. Dragoi, V. Hulea, T. Cacciaguerra, D. Meloni, V. Solinas, E. Dumitriu, *Microporous Mesoporous Mater*. **2012**, *163*, 51-64.

31. P. Selvam, N.V. Krishna, A. Sakthivel, *Adv. Porous Mater*. **2013**, *1*, 239-254.

32. J. Li, L.L. Lou, Y. Yang, H. Hao, S. Liu, *Microporous Mesoporous Mater*. **2015**, *207*, 27-32.

33. S.R. Kirumakki, N. Nagaraju, S. Narayanan, *Appl. Catal. A: Gen*. **2004**, *273*, 1-9.

34. Srivastava, R.; Choi, M.; Ryoo, R. *Chem. Commun.* **2006**, *41*, 4489–4491.

35. P. Rani, R. Srivastava, *ACS Sustain. Chem. Eng.* **2019**, *7*, 9822–9833.

36. J. Bedard, H. Chiang, A. Bhan, *J. Catal*. **2012**, *290*, 210-219.

37. H. Chiang, A. Bhan, *J. Catal*. 2010, *271*, 251-261.

38. M. Krishnamurthy, K. MSM, C. K. Krishnan, *Microporous Mesoporous Mater*. **2016**, *221*, 23-31.

39. Y. Goto, Y. Fukushima, P. Ratu, Y. Imada, Y. Kubota, Y. Sugi, M. Ogura, M. Matsukata, *J. Porous Mater*. **2002**, *9*, 43-48.

40. F. Rouquerol, J. Rouquerol, B. Imelik, *Bull. Soc. Chim. France* **1964**, 635-639.

41. A. Galarneau, L. Desmurs, C. Vaulot, H. Nouali, B. Lebeau, T.J. Daou, V. Hulea, C. Cammarano, I. Batonneau-Gener, A. Sachse, *Catalysis Research*, LIDSEN Publishing Inc, **2022**, *2*, p. 29.

42. J. C. P. Broekhoff, J. H. de Boer, *J. Catal*. **1968**, *10*, 377–390.

43. V. Zholobenko, C. Freitas, M. Jendrlin, P. Bazin, A. Travert, F. Thibault-Starzyk, J. Catal., **2020**, *385*, 52-60.

Table 1. Textural and acidic properties of ZSM5-MT(x) catalysts. Comparison with parent ZSM-5 and Al-MCM-41.

Catalysts	D_{mes}	S_{BET}	S_{mic}	$S_{mes+ext}$	V_{mic}	V_{mes}	FTIR/Pyridine		
	nm	$m^2\ g^{-1}$	$m^2\ g^{-1}$	$m^2\ g^{-1}$	$mL\ g^{-1}$	$mL\ g^{-1}$	Brønsted	Lewis	Total
							$mmol\ g^{-1}$	$mmol\ g^{-1}$	$mmol\ g^{-1}$
ZSM-5	-	372	320	53	0.162	0	0.47	0.11	0.58
ZSM5-MT(0.30)	4.1	443	310	170	0.154	0.128	0.29	0.17	0.46
ZSM5-MT(0.38)	4.1	477	270	170	0.135	0.133	0.27	0.18	0.45
ZSM5-MT(0.50)	4.1	486	250	250	0.122	0.209	0.25	0.18	0.43
ZSM5-MT(0.60)	4.1	533	218	315	0.108	0.257	0.16	0.16	0.32
ZSM5-MT(0.70)	4.1	548	133	415	0.068	0.342	0.15	0.09	0.24
Al-MCM-41	4.0	846	0	850	0	0.72	0.05	0.21	0.26

Table 2. Acidity strength of ZSM5-MT(x) catalysts determined by TPD-NH_3: temperature of desorption of the two peaks of TPD-NH_3 spectra and amount of associated acid sites. Comparison with parent ZSM-5 and Al-MCM-41.

Catalysts	T_1	T_2	Q_1	Q_2	Q_{total}
	K	K	$mmol\ g^{-1}$	$mmol\ g^{-1}$	$mmol\ g^{-1}$
ZSM-5	475	693	0.64	0.21	0.85
ZSM5-MT(0.30)	471	693	0.45	0.19	0.64
ZSM5-MT(0.38)	471	693	0.34	0.16	0.50
ZSM5-MT(0.50)	471	663	0.30	0.16	0.46
ZSM5-MT(0.60)	460	643	0.24	0.16	0.40
ZSM5-MT(0.70)	460	623	0.12	0.13	0.25
Al-MCM-41	441	523	0.24	0.16	0.40

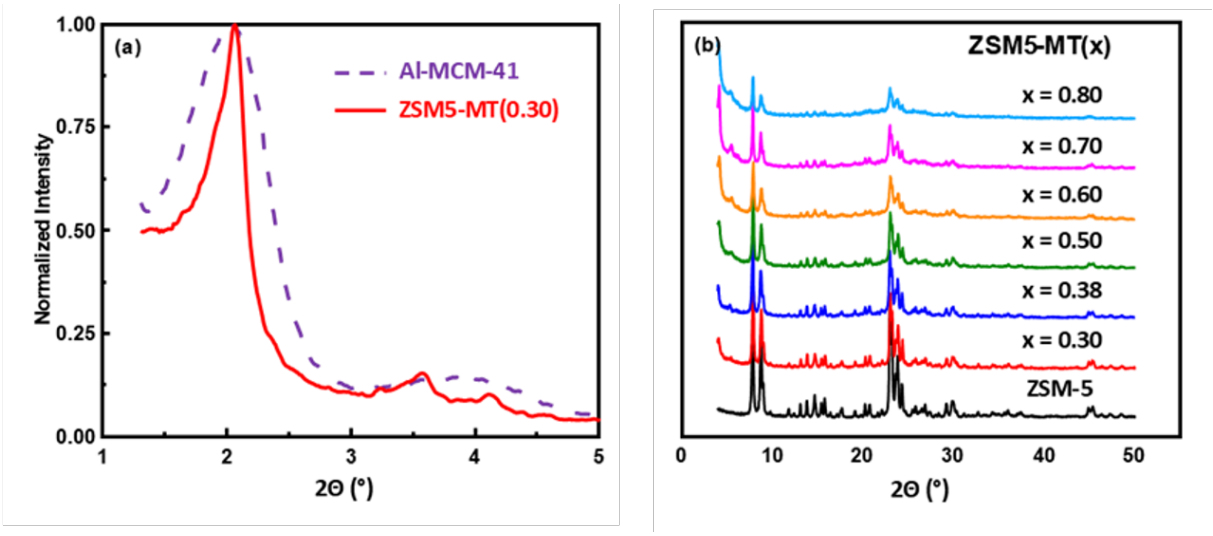

Figure 1. XRD pattern of ZSM5-MT(x) at (a) low and (b) large angles. As comparison XRD pattern of Al-MCM-41 and parent ZSM-5 are given. For sake of clarity, only low angle XRD pattern of ZSM5-MT(0.3) is given, the other ZSM5-MT(x) are shown in Figure S1.

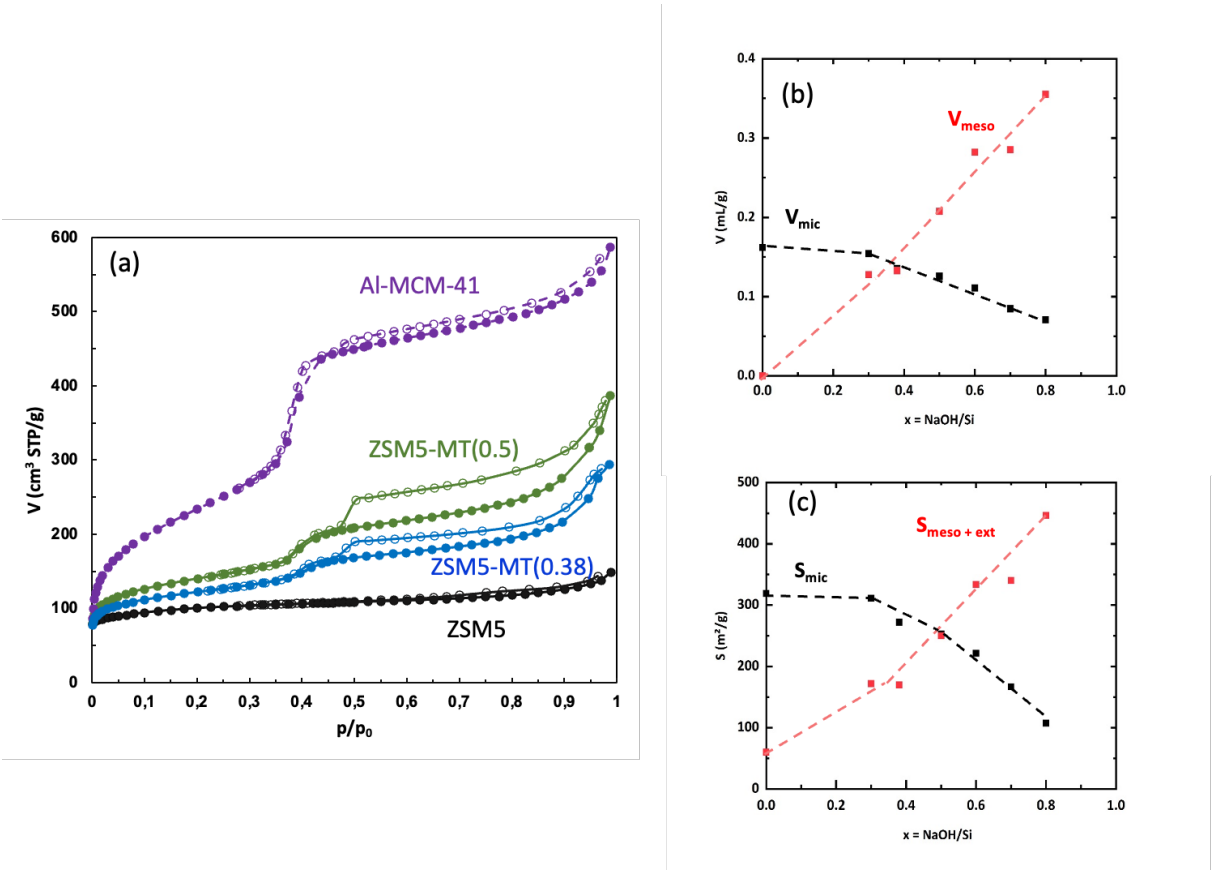

Figure 2. (a) Nitrogen sorption isotherms at 77 K of pristine ZSM-5, ZSM5-MT(x) and Al-MCM-41 (plain symbols for the adsorption and empty symbols for the desorption). (b) Micropore and mesopore volume and (c) micropore surface area and mesopore plus external surface area of ZSM-5-MT(x) determined by the corrected *t*-plot method. For sake of clarity, only isotherms of ZSM5-MT(x) with x = 0.38 and 0.5 are given, the other isotherms of ZSM5-MT(x) are shown in Figure S1.

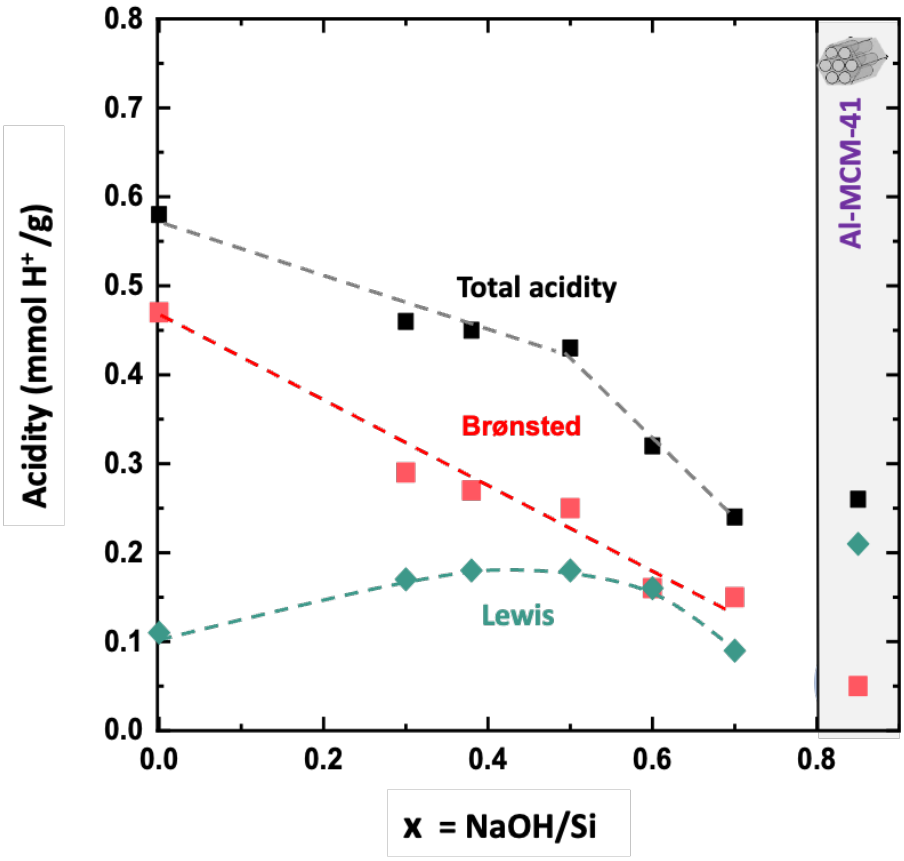

Figure 3. Evolution of the number of acid sites (Brønsted, Lewis, Total) determined by FTIR/pyridine (after outgassing at 423 K) as a function of x for ZSM5-MT(x). As comparison results for parent ZSM-5 (at x = 0) and Al-MCM-41 are given.

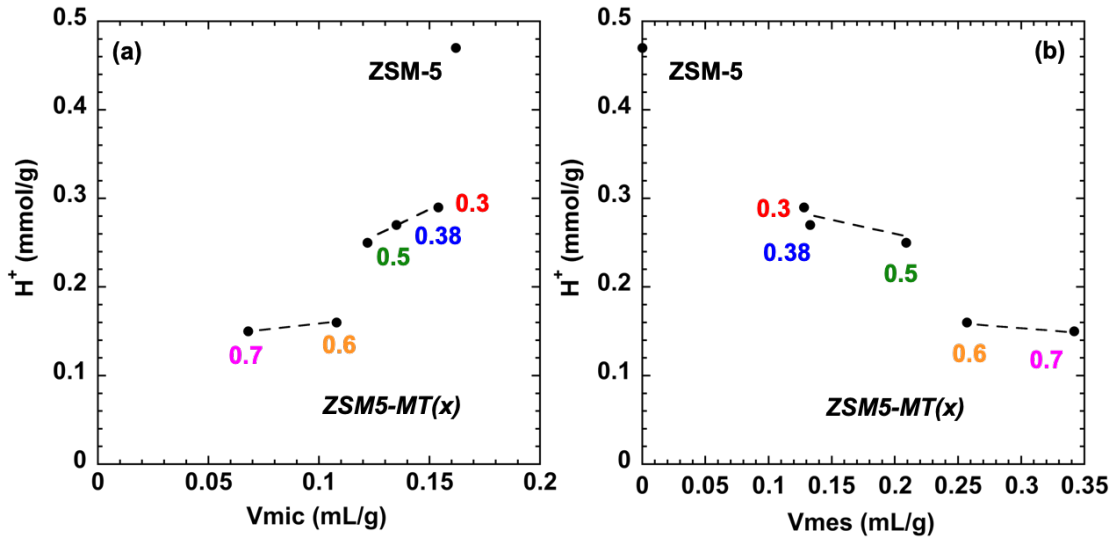

Figure 4. Relationship between the number of Brønsted acid sites and the micro- or mesoporous volume of ZSM5-MT(x) catalysts. The x values are indicated in the Figure.

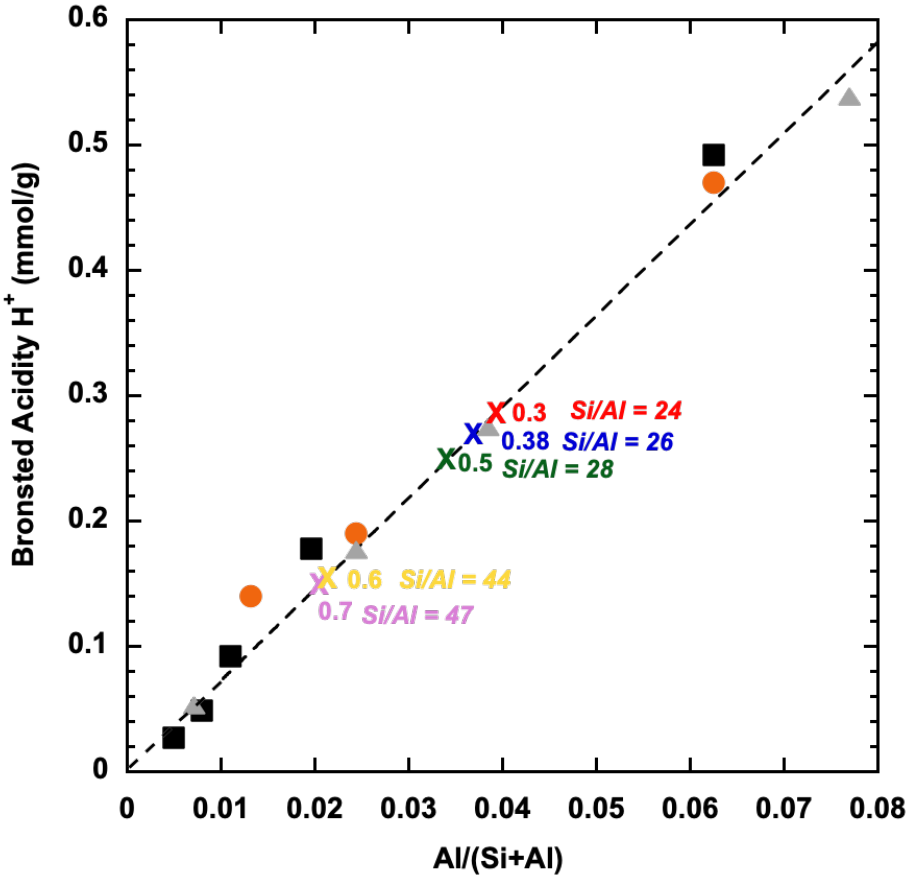

Figure 5. Relationship between the number of Brønsted acid sites in ZSM-5 catalysts of different Si/Al ratio as a function of their number of Al in the structure. The dashed line represents the fit of the data (Eq. 1). From the fit corresponding Si/Al ratio of of ZSM5-MT(x) catalysts for x = 0.3, 0.38, 0.5, 0.6, 0.7 have been calculated. Data from (orange circles) this work, (black square) from ref. 25, (grey triangle) from ref. 26.

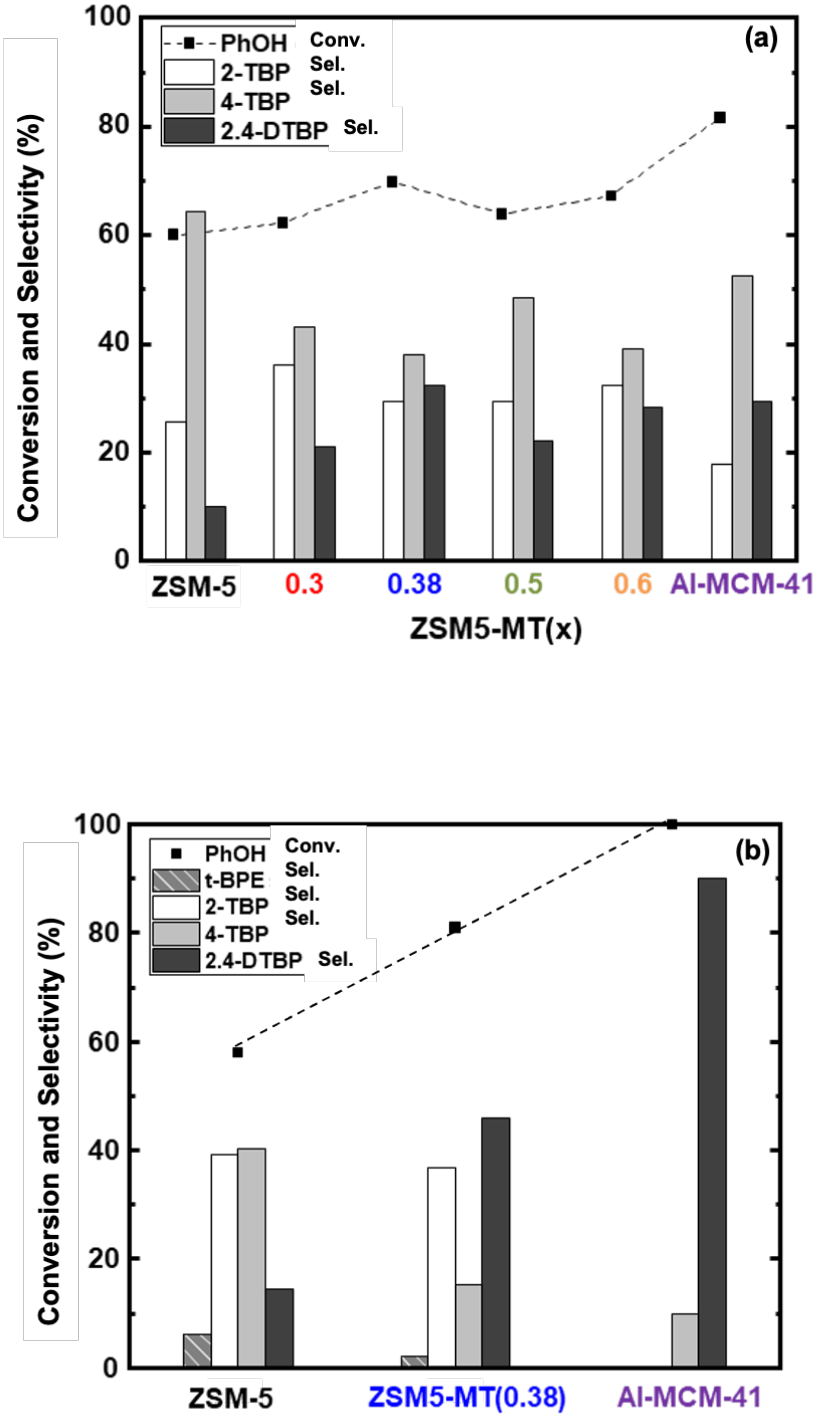

Figure 6. Results of the alkylation of phenol by *t*-BuOH over parent ZSM-5, ZSM5-MT(x) and Al-MCM-41 catalysts at 393 K. Phenol conversion for *t*-BuOH/phenol molar ratio of (blue square and dashed line) 3:1 and (red square and dashed line) 1:1. Selectivity of 2,4-DTBP for *t*-BuOH/phenol molar ratio of (blue bar) 3:1 and (red bar) 1:1.

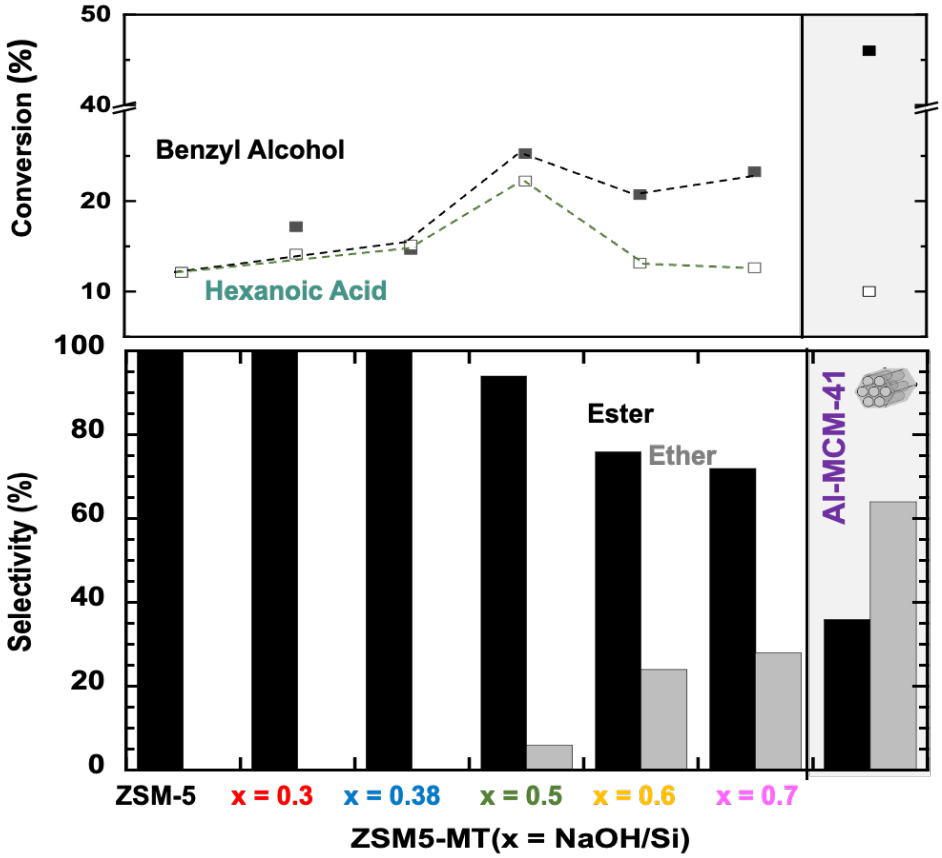

Figure 7. Esterification of benzyl alcohol by hexanoic acid with parent ZSM-5, ZSM5-MT(x) and Al-MCM-41 catalysts. (up) conversion of benzyl alcohol and hexanoic acid, (down) selectivity (black) in benzyl hexanoate and (grey) in benzyl ether.

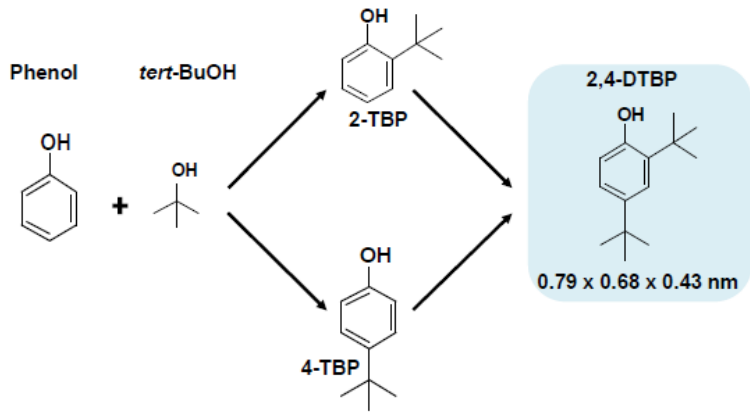

Scheme 1. Main reactions of phenol alkylation with *t*-BuOH

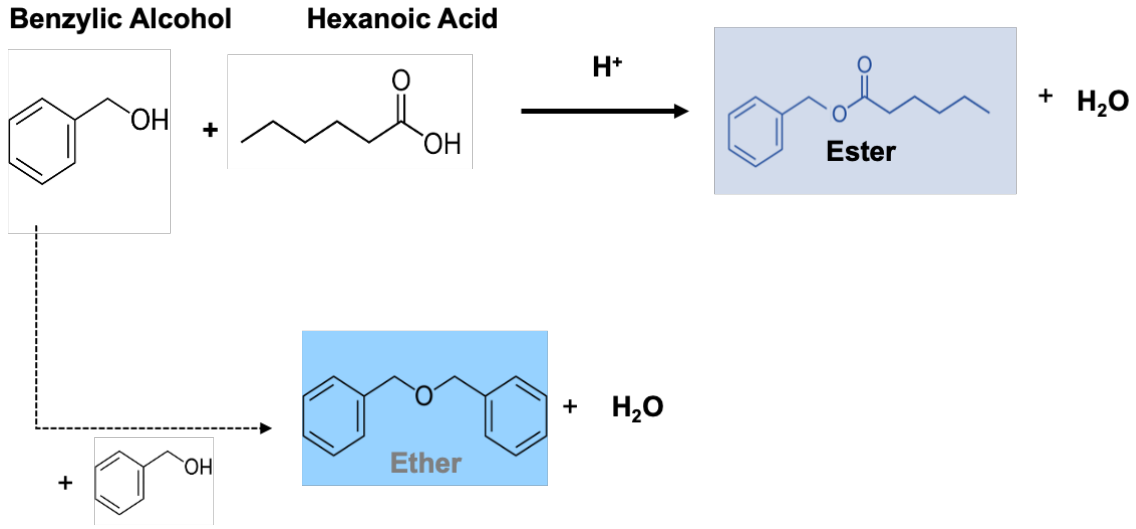

Scheme 2. Esterification of benzyl alcohol with hexanoic acid